J|A|C|S ARTICLES

Published on Web 02/09/2009

Synthesis, Radiolabeling, and Bio-imaging of High-Generation Polyester Dendrimers

Matthew C. Parrott,[†] S. Rahima Benhabbour,[†] Chantal Saab,[||] Jennifer A. Lemon,[‡] Shannon Parker,[‡] John F. Valliant,*[,†,‡] and Alex Adronov*[,†,§]

Department of Chemistry, Medical Physics and Applied Radiation Sciences, McMaster Centre for Preclinical and Translational Imaging, and Brockhouse Institute for Materials Research, McMaster University, Hamilton, Ontario L8S 4M1, Canada

Received October 4, 2008; E-mail: adronov@mcmaster.ca

Ⓦ **This paper contains enhanced objects available on the Internet at http://pubs.acs.org/jacs.**

Abstract: A series of aliphatic polyester dendrons, generations 1 through 8, were prepared with a core *p*-toluenesulfonyl ethyl (TSe) ester as an easily removable protecting group that can be efficiently replaced with a variety of nucleophiles. Using amidation chemistry, a tridentate bis(pyridyl)amine ligand which is known to form stable complexes with both Tc(I) and Re(I) was introduced at the dendrimer core. Metalation of the core ligand with ^{99m}Tc was accomplished for generations 5 through 7, and resulted in regioselective radiolabeling of the dendrimers. The distribution of the radiolabeled dendrimers was evaluated in healthy adult Copenhagen rats using dynamic small-animal single photon emission computed tomography (SPECT). The labeled dendrimers were cleanly and rapidly eliminated from the bloodstream via the kidneys with negligible nonspecific binding to organs or tissues being observed. These data were corroborated by a quantitative biodistribution study on the generation 7 dendrimer following necropsy. The quantitative biodistribution results were in excellent agreement with the data obtained from the dynamic SPECT images.

Introduction

Since the pioneering work of Ringsdorf[1,2] and Kopecek,[3,4] the field of macromolecular therapeutics has received continually increasing attention.[5−9] The advantages of conjugating small-molecule drugs to water-soluble, nontoxic, biocompatible polymers have been repeatedly documented[9−11] and include improved drug solubility, longer blood circulation time, decreased toxicity to healthy cells and tissues, and the possibility to deliver drug payloads specifically to disease sites via both passive[12−14] and active targeting methods.[15,16] Within this area, the dendritic polymer architecture holds significant potential due to a number of decisive advantages.[17−21] The controlled, stepwise synthetic protocols used in dendrimer synthesis enable the formation of precisely defined structures that can be modified at their core, interior branch points, and periphery, allowing introduction of therapeutic agents, targeting moieties, and solubilizing functionalities as necessary. Additionally, the monodisperse nature of dendritic polymers enables facile characterization and eliminates reproducibility issues that may arise when using traditional, polydisperse macromolecular therapeutics that contain polymer fractions with greatly differing molecular weights.[22]

Among the wide array of dendrimer structures that have been reported over the past four decades, several have been heavily investigated for biological/therapeutic applications.[22−25] The commercially available polyamidoamine and polypropyleneimine dendrimers have been most widely studied, especially in gene delivery, as MRI contrast agents, and as covalent drug conjugates.[26] The more biocompatible peptide-based dendrimers

[†] Department of Chemistry.
[‡] Medical Physics and Applied Radiation Sciences.
[||] McMaster Centre for Preclinical and Translational Imaging.
[§] Brockhouse Institute for Materials Research.

(1) Ringsdorf, H. *J. Polym. Sci., Polym. Symp.* **1975**, 135–153.
(2) Bader, H.; Ringsdorf, H.; Schmidt, B. *Angew. Makromol. Chem.* **1984**, *123*, 457–485.
(3) Kopecek, J. *Polym. Med.* **1977**, *7*, 191–221.
(4) Kopecek, J.; Kopeckova, P.; Minko, T.; Lu, Z. R. *Eur. J. Pharm. Biopharm.* **2000**, *50*, 61–81.
(5) Duncan, R. *Nat. Rev. Drug Discovery* **2003**, *2*, 347–360.
(6) Kopecek, J.; Kopeckova, P.; Minko, T.; Lu, Z. R. *Eur. J. Pharm. Biopharm.* **2000**, *50*, 61–81.
(7) Twaites, B.; Alarcon, C. D.; Alexander, C. *J. Mater. Chem.* **2005**, *15*, 441–455.
(8) Pasut, G.; Veronese, F. *Prog. Polym. Sci.* **2007**, *32*, 933–961.
(9) Park, J. H.; Lee, S.; Kim, J.; Park, K.; Kim, K.; Kwon, I. C. *Prog. Polym. Sci.* **2008**, *33*, 113–137.
(10) Kopecek, J.; Kopeckova, P.; Minko, T.; Lu, Z. R.; Peterson, C. M. *J. Controlled Release* **2001**, *74*, 147–158.
(11) Jensen, K. D.; Nori, A.; Tijerina, M.; Kopeckova, P.; Kopecek, J. *J. Controlled Release* **2003**, *87*, 89–105.
(12) Matsumura, Y.; Maeda, H. *Cancer Res.* **1986**, *46*, 6387–6392.
(13) Maeda, H.; Seymour, L. W.; Miyamoto, Y. *Bioconjugate Chem.* **1992**, *3*, 351–362.
(14) Maeda, H.; Wu, J.; Sawa, T.; Matsumura, Y.; Hori, K. *J. Controlled Release* **2000**, *65*, 271–284.
(15) Khandare, J.; Minko, T. *Prog. Polym. Sci.* **2006**, *31*, 359–397.
(16) Lu, Z. R.; Shiah, J. G.; Sakuma, S.; Kopeckova, P.; Kopecek, J. *J. Controlled Release* **2002**, *78*, 165–173.
(17) Frechet, J. M. J. *Science* **1994**, *263*, 1710–1715.
(18) Bosman, A. W.; Janssen, H. M.; Meijer, E. W. *Chem. Rev.* **1999**, *99*, 1665–1688.
(19) Frechet, J. M. J.; Tomalia, D. A. *Dendrimers and Other Dendritic Polymers*; John Wiley & Sons, Ltd.: West Sussex, 2001.
(20) Frechet, J. M. J. *J. Polym. Sci. Polym. Chem.* **2003**, *41*, 3713–3725.
(21) Tomalia, D. A. *Prog. Polym. Sci.* **2005**, *30*, 294–324.
(22) Gillies, E. R.; Frechet, J. M. J. *Drug Discovery Today* **2005**, *10*, 35–43.

10.1021/ja8078175 CCC: $40.75

have also been demonstrated to exhibit promising characteristics as components of vaccines, as well as antiviral and antibacterial agents.[27] In addition, polyester dendrimers have been applied to tissue engineering and surgical closure materials, where they have been used as degradable photo-cross-linkers for repairing corneal wounds.[28] More recently, aliphatic polyester dendrimers based on the 2,2-bis(hydroxymethyl)propanoic acid (bis-MPA) building block have been studied as potential drug-delivery agents.[29,30] These poly(2,2-bis(hydroxymethyl)propanoic acid) (PMPA) dendrimer structures, initially reported by Ihre and Hult,[31,32] uniquely exhibit excellent aqueous solubility, low *in vivo* toxicity, biocompatibility, and biodegradability while being relatively easy to fabricate via convergent[31] or divergent methods.[33] Thus, these structures have been modified to incorporate various therapeutic agents within their interior[34] and on their periphery.[22,29,35,36] Furthermore, peripheral functionalization of PMPA polyester dendrimers with high-molecular-weight poly(ethylene oxide) (PEO) chains has been found to result in long blood residence times for the dendrimer−PEO conjugates.[37] Recently, Fréchet and co-workers have demonstrated that "bow-tie" PMPA dendrimer conjugates with doxorubicin (DOX) exhibit high tumor uptake and greatly diminished cytotoxicity (relative to free DOX).[37,38] These compounds were found to completely eradicate colon carcinoma in mice after a single intravenous injection.[39] The use of PMPA dendrimer structures in therapeutic applications is therefore becoming more prominent.

In these and all other examples of macromolecular therapeutic agents, biodistribution studies that detail both pharmacokinetics and pharmacodynamics are critical in assessing the efficacy of the therapeutic agent. Typically, this is accomplished using iodine-125 (^{125}I) to radioiodinate phenol-functionalized derivatives of the target therapeutic agent.[37,40−42] However, introduction of the requisite radio-iodinated phenols can result in enhanced liver uptake,[39] providing an inaccurate biodistribution picture of the target. Additionally, the biodistribution studies of ^{125}I-labeled compounds is generally suited for *ex vivo* radioactivity measurement within harvested organs or the "cut and count" methodology, which provides a "snapshot" of the distribution and requires large numbers of animals to get dynamic and statistically relevant data. Conversely, radio-imaging agents are routinely used in diagnostic medicine to locate and follow the progression of disease as well as to monitor organ function *in vivo* and in real-time.[43] The exquisite sensitivity and temporal resolution of radio-imaging methodologies make them extremely useful not only in diagnostic medicine but also in determining the distribution and kinetics of novel radiolabeled compounds in preclinical and clinical studies.

Of all the known radionuclides, the γ-emitting ^{99m}Tc is the most commonly used medical isotope in diagnostic medicine due to its ideal half-life (6 h) and γ-energy (140 keV), low dose burden to patients, and the widespread availability of low-cost ^{99}Mo/^{99m}Tc-generators.[44] Specifically, these properties of ^{99m}Tc make it the preferred radionuclide in single photon emission computed tomography (SPECT), a radio-imaging methodology that enables real-time, *in vivo* determination of the distribution that a γ-emitting radionuclide traverses post injection into a human or animal subject. Despite the widespread use of ^{99m}Tc,[44] its use in determining the pharmacokinetics and pharmacodynamics of macromolecular drug delivery agents has received very little attention. To the best of our knowledge, there are only two prior publications involving the chelation of ^{99m}Tc within dendrimers, but neither extends the dendrimer−^{99m}Tc complexes to radio-imaging.[45,46] In addition, the multisite, poorly controlled binding of the radionuclide within these reported dendrimers diminishes their clinical applicability and overall utility in diagnostic imaging.

One approach to preparing a well-defined and robust ^{99m}Tc-labeled dendrimer that is suitable for SPECT imaging is to incorporate a single high-affinity Tc ligand at the core of a high-generation dendrimer. This would ensure that radiolabeling occurs in a well-defined, site-specific manner and at only a single point within the dendrimer framework. Furthermore, by introducing the radionuclide at the site-isolated core of the dendrimer, the overall size, shape, polarity, and mode of interaction of the dendrimer periphery with its external environment should not be appreciably affected. Therefore, the biodistribution of the radiolabeled dendrimer should mimic that of an unlabeled analogue. To accomplish this, an orthogonal protecting group that can be dendronized in a divergent manner was utilized to produce core-protected, high-generation, biocompatible PMPA dendrimers. This protecting group can subsequently be selectively cleaved in high yield at any generation to liberate a single, accessible carboxylic acid group. Amidation of the deprotected core with an aminoalkyl-functionalized bis(pyridyl)amine ligand allowed the introduction of an extremely efficient single-site chelator for ^{99m}Tc.[47] Herein, we describe the synthesis of these

(23) Boas, U.; Heegaard, P. *Chem. Soc. Rev.* **2004**, *33*, 43.
(24) Tomalia, D. A.; Reyna, L. A.; Svenson, S. *Biochem. Soc. Trans.* **2007**, *35*, 61–67.
(25) Svenson, S.; Tomalia, D. A. *Adv. Drug Delivery Rev.* **2005**, *57*, 2106–2129.
(26) Cheng, Y.; Gao, Y.; Rao, T.; Li, Y.; Xu, T. *Comb. Chem. High Throughput Screening* **2007**, *10*, 336–349.
(27) Crespo, L.; Sanclimens, G.; Pons, M.; Giralt, E.; Royo, M.; Albericio, F. *Chem. Rev.* **2005**, *105*, 1663–1681.
(28) Grinstaff, M. W. *Chem.-Eur. J.* **2002**, *8*, 2838–2846.
(29) Ihre, H. R.; De Jesus, O. L. P.; Szoka, F. C.; Frechet, J. M. J. *Bioconjugate Chem.* **2002**, *13*, 443–452.
(30) De Jesus, O. L. P.; Ihre, H. R.; Gagne, L.; Frechet, J. M. J.; Szoka, F. C. *Bioconjugate Chem.* **2002**, *13*, 453–461.
(31) Ihre, H.; Hult, A.; Frechet, J. M. J.; Gitsov, I. *Macromolecules* **1998**, *31*, 4061–4068.
(32) Ihre, H.; Hult, A.; Soderlind, E. *J. Am. Chem. Soc.* **1996**, *118*, 6388–6395.
(33) Ihre, H.; De Jesus, O. L. P.; Frechet, J. M. J. *J. Am. Chem. Soc.* **2001**, *123*, 5908–5917.
(34) Parrott, M. C.; Marchington, E. B.; Valliant, J. F.; Adronov, A. *J. Am. Chem. Soc.* **2005**, *127*, 12081–12089.
(35) Lee, C. C.; MacKay, J. A.; Frechet, J. M. J.; Szoka, F. C. *Nat. Biotechnol.* **2005**, *23*, 1517–1526.
(36) Malik, N.; Evagorou, E. G.; Duncan, R. *Anti-Cancer Drug* **1999**, *10*, 767–776.
(37) Gillies, E. R.; Dy, E.; Fréchet, J. M. J. F.; Szoka, F. C. *Mol. Pharmaceutics* **2005**, *2*, 129–138.
(38) Gillies, E. R.; Fréchet, J. M. J. *J. Am. Chem. Soc.* **2002**, *124*, 14137–14146.
(39) Lee, C. C.; Gillies, E. R.; Fox, M. E.; Guillaudeu, S. J.; Frechet, J. M. J.; Dy, E.; Szoka, F. C. *Proc. Natl. Acad. Sci. U.S.A.* **2006**, *103*, 16649.
(40) Malik, N.; Wiwattanapatapee, R.; Klopsch, R.; Lorenz, K.; Frey, H.; Weener, J. W.; Meijer, E. W.; Paulus, W.; Duncan, R. *J. Controlled Release* **2000**, *65*, 133–148.
(41) Lee, C. C.; Yoshida, M.; Frechet, J. M. J.; Dy, E. E.; Szoka, F. C. *Bioconjugate Chem.* **2005**, *16*, 535–541.
(42) Larwood, D. J.; Szoka, F. C. *J. Labelled Compd. Radiopharm.* **1984**, *21*, 603–614.
(43) Britz-Cunningham, S. H.; Adelstein, S. J. *J. Nucl. Med.* **2003**, *44*, 1945–1961.
(44) Abram, U.; Alberto, R. *J. Brazil Chem. Soc.* **2006**, *17*, 1486–1500.
(45) Stephan, H.; Spies, H.; Johannsen, B.; Gloe, K.; Gorka, M.; Vogtle, F. *Eur. J. Inorg. Chem.* **2001**, 2957–2963.
(46) Agashe, H.; Babbar, A.; Jain, S.; Sharma, R.; Mishra, A.; Asthana, A.; Garg, M.; Dutta, T.; Jain, N. *Nanomedicine: Nanotechnol., Biol. Med.* **2007**, *3*, 120–127.

Scheme 1

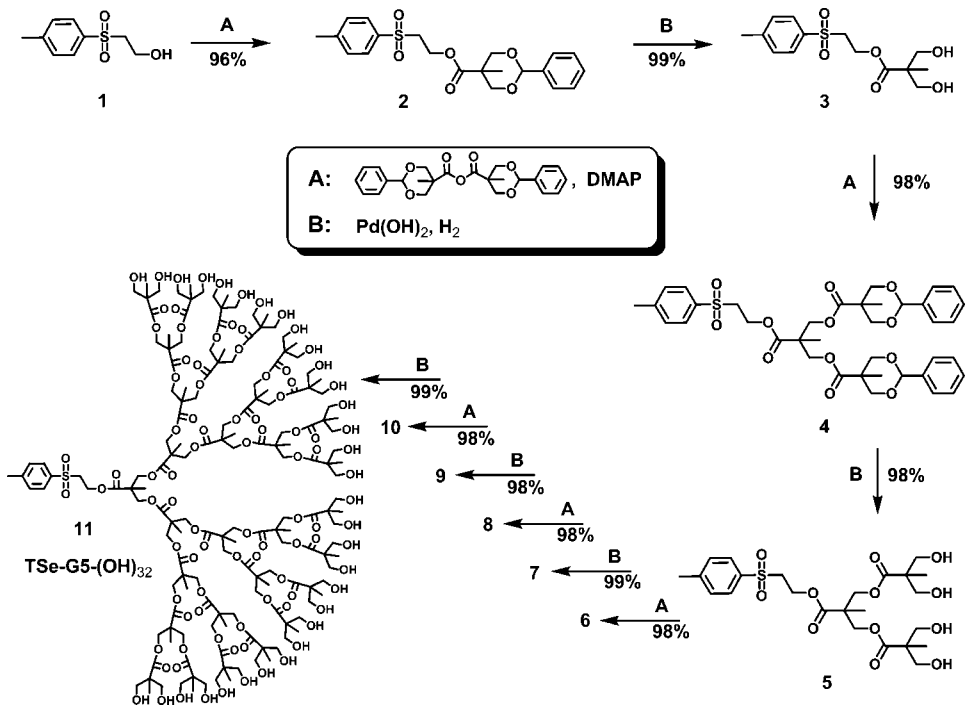

ligand-bearing dendrimers, their labeling with ^{99m}Tc in high radiochemical yield, and preliminary *in vivo* SPECT imaging results obtained with a series of high-generation radiolabeled dendrimers. This work represents early stages in the development of a dendrimer family that can house a therapeutic payload, be targeted to specific disease sites through peripheral modification, and be monitored in real-time upon injection into, perfusion through, and elimination from preclinical models and, ultimately, patients.

Results and Discussion

General Synthesis. To produce PMPA dendrons in which the core could be modified at a later stage, it was necessary to first identify a protecting group for the carboxylic acid functionality that is stable to the dendrimer synthesis chemistry and could be efficiently removed under orthogonal conditions. After surveying a number of possibilities, we settled on the toluenesulfonyl ethyl (TSe) ester as a viable candidate because of its stability toward dendron growth/deprotection conditions and its facile cleavage using the non-nucleophilic base 1,8-diazabicyclo[5.4.0]undec-7-ene (DBU).[48] The synthesis of our desired dendrons was therefore accomplished by initially reacting *p*-toluenesulfonyl ethanol (**1**) with the benzylidene-protected anhydride of bis-MPA[33] using a catalytic amount 4-dimethylaminopyridine. The excess anhydride was quenched with water, and the first-generation (G1) TSe-protected dendron (**2**) was obtained in 96% isolated yield after a simple extraction (Scheme 1). For the subsequent dendrimer growth reactions, it was found that using a 3:2 mixture of CH_2Cl_2 and pyridine and a 2-fold excess of the bis-MPA anhydride relative to each alcohol functionality constituted optimal conditions for all generations. The benzylidene protecting group of **2** was quantitatively removed by hydrogenolysis using a catalytic amount of 20% (w/w) $Pd(OH)_2/C$ and H_2 (1 atm) to produce the diol **3**. Subsequent iterations of these steps (Scheme 1) allowed the production of a series of hydroxyl-terminated dendrons, from G1 to G8, with isolated yields in excess of 90% up to the eighth generation. For simplicity, we refer to the different members of each dendron generation according to the core functionality (TSe, COOH, etc.), the dendron generation (G*x*), and the peripheral groups (O_2Bn or OH). Therefore, the fifth-generation dendron (**11**) in Scheme 1 is referred to as TSe-G5-$(OH)_{32}$ and contains one core TSe moiety and 32 peripheral hydroxyls. Each of these dendron structures was fully characterized by ^{1}H and ^{13}C NMR as well as MALDI-TOF mass spectrometry. The MALDI-TOF mass spectra of TSe-G5-$(OH)_{32}$ (3798 Da), TSe-G6-$(OH)_{64}$ (7511 Da), TSe-G7-$(OH)_{128}$ (14 938 Da), and TSe-G8-$(OH)_{256}$ (29 792 Da) are depicted in Figure 1, showing observed signals that correspond to the sodium adducts of each of the dendrons.

The fourth- to eighth-generation fully protected dendrons were also characterized by size exclusion chromatography (SEC),

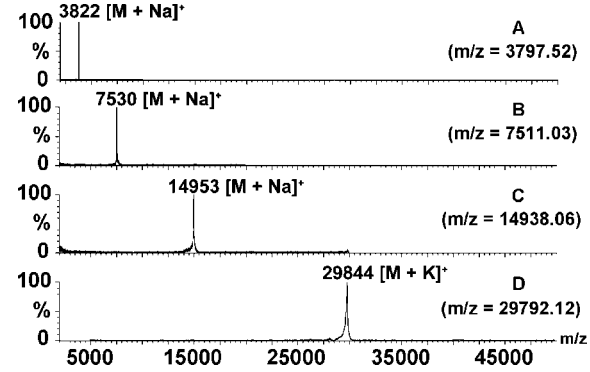

Figure 1. MALDI-TOF MS spectra of compounds TSe-G5-$(OH)_{32}$ (A), TSe-G6-$(OH)_{64}$ (B), TSe-G7-$(OH)_{128}$ (C), and TSe-G8-$(OH)_{256}$ (D).

(47) Banerjee, S. R.; Levadala, M. K.; Lazarova, N.; Wei, L. H.; Valliant, J. F.; Stephenson, K. A.; Babich, J. W.; Maresca, K. P.; Zubieta, J. *Inorg. Chem.* **2002**, *41*, 6417–6425.

(48) Greene, T. W.; Wuts, P. G. W. *Protective Groups in Organic Synthesis*, 3rd ed.; Wiley-Interscience: New York, 1999.

Table 1. Molecular Weight and Hydrodynamic Radius Data for the G4−G8 Fully Protected Dendrons

		SEC (TDA)			
compound	theor mol wt	M_n	PDI	MS mol wt[a]	R_h (nm)
TSe-G4-$(O_2Bn)_8$	2 645	2 860	1.003	2 665	1.15
TSe-G5-$(O_2Bn)_{16}$	5 206	6 480	1.004	5 215	1.42
TSe-G6-$(O_2Bn)_{32}$	10 328	10 900	1.047	10 353	1.82
TSe-G7-$(O_2Bn)_{64}$	20 572	23 460	1.031	20 593	2.27
TSe-G8-$(O_2Bn)_{128}$	41 060	47 570	1.019	41 152	2.80

[a] Data acquired by MALDI-TOF MS, except for G4, which was acquired by electrospray ionization MS. All MALDI signals correspond to the Na or K adduct of the molecular ion.

coupled with viscometry and light-scattering data (using a Viscotek Triple Detector Array-301 system). The combination of a mass detector (refractive index) with a viscometer and light-scattering detector enables the characterization of polymers having diverse compositions and architectures, without the inaccuracies that plague typical SEC systems calibrated with specific polymer standards. The molecular weight data measured with the triple detector array are given in Table 1, and are consistent with the expected doubling on going from one generation to the next. Narrow polydispersities were observed at each generation, in reasonable agreement with the MALDI-TOF data that indicate pure compounds of exact molecular weight. It is important to also note the hydrodynamic radii (R_h) of these structures. Although the R_h values steadily increased with generation, they were all well below 3 nm, even for the relatively high-generation dendrimers.

Removal of the TSe protecting group was performed on G5 through G8 by reacting each dendron with an excess of DBU in dichloromethane (DCM). Thin-layer chromatography (TLC) of this reaction indicated complete disappearance of starting materials within 1 h; however, the reaction was allowed to continue for an additional 12 h to ensure quantitative removal of the TSe group. The resulting dendrons were washed with $NaHSO_4$ (1 M) to remove the excess DBU and precipitated three times in 9:1 hexanes:ethyl acetate. Deprotection of the internal TSe ester was confirmed by ^{1}H NMR spectroscopy, where a complete disappearance of the aromatic signal at 7.8 ppm (2H) as well as the aliphatic proton signals at 2.5 ppm (3H) and 3.3 ppm (2H) was observed for each generation (see example spectra for the G5 dendron in Figure 2). In addition, the MALDI mass spectrum for COOH-G5-$(O_2Bn)_{16}$ shows the removal of the TSe moiety, with a mass decrease of the expected 185 Da from the original mass of TSe-G5-$(O_2Bn)_{16}$ (Figure 3). Identical mass decreases were observed for the higher generation dendrons.

The benzylidene protecting groups of COOH-G5-$(O_2Bn)_{16}$ were quantitatively removed using the aforementioned hydrogenolysis conditions to produce the COOH-G5-$(OH)_{32}$ dendron with one internal carboxylic acid and 32 peripheral alcohols (Scheme 2). The ^{1}H NMR spectrum of COOH-G5-$(OH)_{32}$, depicted in Figure 2, confirms the deprotection of the benzylidene groups by the complete disappearance of aromatic signals at 7.2−7.4 ppm as well as the disappearance of the acetal proton on each benzylidene at 5.5 ppm (16 H). Note that the ^{1}H NMR spectrum of the fully deprotected dendron, COOH-G5-$(OH)_{32}$, was recorded in deuterated methanol (as opposed to $CDCl_3$), which accounts for the observed shifts in all signals, as well as the appearance of extra signals at 3.31 and 4.87 ppm, due to the presence of methanol and water, respectively. Additionally, the MALDI-MS data show the complete conversion of COOH-G5-$(O_2Bn)_{16}$ to COOH-G5-$(OH)_{32}$ by the decrease in observed mass from 5030 to 3636 Da (Figure 3).

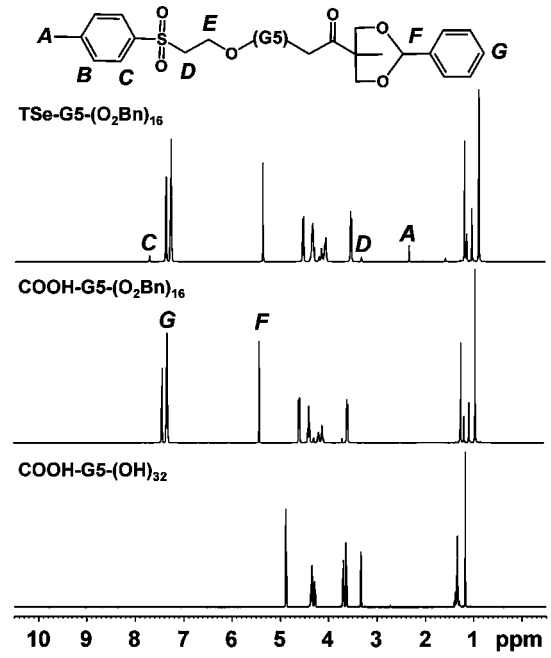

Figure 2. ^{1}H NMR spectra of TSe-G5-$(O_2Bn)_{16}$ (in $CDCl_3$), COOH-G5-$(O_2Bn)_{16}$ (in $CDCl_3$), and COOH-G5-$(OH)_{32}$ (in CD_3OD).

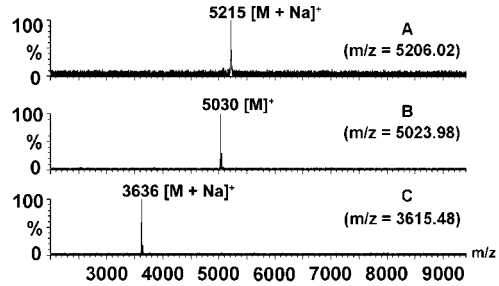

Figure 3. MALDI-TOF spectra of TSe-G5-$(O_2Bn)_{16}$ (A), COOH-G5-$(O_2Bn)_{16}$ (B), and COOH-G5-$(OH)_{32}$ (C).

Identical deprotection chemistry procedures were successfully applied to the higher generation dendrons with no significant decrease in yields (see Supporting Information for complete experimental details).

Synthesis of a Bifunctional Bis(pyridyl)amine Ligand for ^{99m}Tc. Having achieved the preparation of high-generation dendrons with a reactive acid functionality at the core, it became possible to introduce a ligand for ^{99m}Tc. As stated above, placement of the ligand at the dendrimer core was considered critical to minimizing the impact of radionuclide introduction on the interactions of the macromolecule with its biological environment during blood and tissue circulation. Site isolation of functional groups within the interior of high-generation dendrimers is a well-known phenomenon[49] and was expected to minimize any impact of the metal complex on overall biodistribution. Additionally, it was important for the linkage between the ligand and the dendron to be robust under physiological conditions, so as to ensure that the radionuclide would not be cleaved prematurely from the dendron during the radio-imaging experiments. An amide linkage to the acid core was therefore preferable to the more labile ester linkage.

Having identified these requirements, we chose to prepare the bifunctional compound **13** (Scheme 3), bearing a free amine

(49) Hecht, S.; Frechet, J. M. J. *Angew. Chem., Int. Ed.* **2001**, *40*, 74–91.

Scheme 2

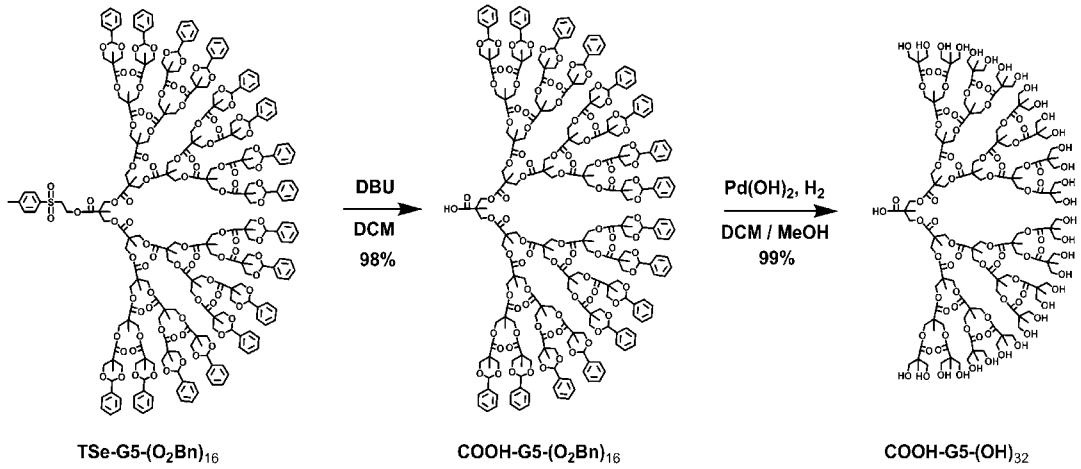

Scheme 3

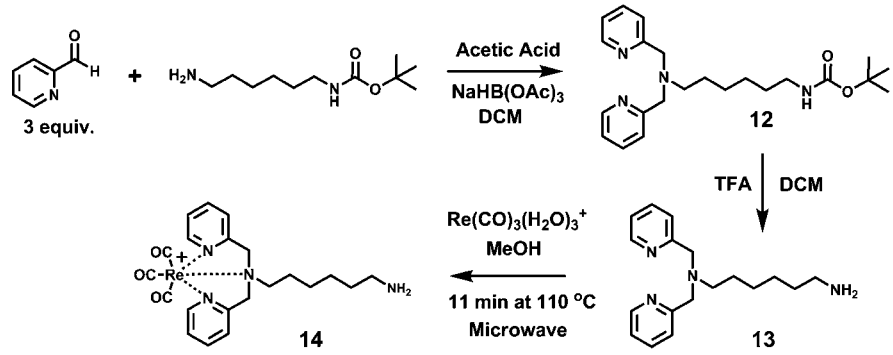

at one end and a bis(pyridyl)amine metal-chelating moiety at the other. The free primary amine of **13** could be coupled to the internal carboxylic acid of our aliphatic polyester dendrons at any generation, and the bis(pyridyl)amine metal chelator could coordinate ^{99m}Tc, as well as its nonradioactive congenor rhenium, which is used as a reference standard.

The preparation of the bifunctional ligand was achieved by reductive amination of 2-pyridylcarboxaldehyde with commercially available *tert*-butyl *N*-(6-aminohexyl)carbamate hydrochloride in a mixture of acetic acid and dry dichloromethane.[50] Upon mixing these components and stirring for 30 min, excess sodium triacetoxy borohydride was added and allowed to react for an additional 3 h to produce the t-BOC-protected aminoalkyl-functionalized bis(pyridyl)amine ligand **12** (Scheme 3). The t-BOC moiety was removed by treatment with trifluoroacetic acid, and ligand **13** was extensively purified by preparative HPLC to ensure a high degree of purity for subsequent coupling and metalation steps. Standard column chromatography proved inadequate for purifying this highly polar ligand to the extent required for radiotracer development.

In order to test conditions for the metalation chemistry with the bifunctional ligand **13**, and to produce a nonradioactive analogue of the desired ^{99m}Tc complex as an HPLC standard, ligand **13** was reacted with $[Re(CO)_3(H_2O)_3]^+$ in methanol under microwave irradiation for 11 min at 110 °C, followed by workup and purification by preparative HPLC to produce the Re complex **14**. The ^{1}H NMR spectra of compounds **13** and **14** are depicted in Figure 4. These spectra clearly indicate that successful metalation had occurred, as can be seen from the shift and splitting of the proton signal at 3.82 ppm (4H) to two new signals at 4.41 ppm (2H) and 5.83 ppm (2H). These new signals appear as a result of the ring structure that is formed upon Re chelation, forcing the pyridyl methylene protons to occupy either axial or equatorial positions, leading to two distinct signals. In addition, a dramatic shift of the signal at 2.65 ppm to 3.73 ppm, as well as smaller downfield shifts of the aromatic pyridyl protons (7.24, 7.85, and 8.68 ppm), indicated that the electronic environment around the pyridine rings and the tertiary amine had also changed.

Amidation with the Dendron Core. At this point, the coupling chemistry between the bifunctional ligand (**13**) and the dendron core was investigated. Amidation of **13** with COOH-G5-$(O_2Bn)_{16}$ to yield the fifth-generation ligand-functionalized dendrimer proceeded smoothly using *o*-benzotriazole-*N*,*N*,*N*′,*N*′,-tetramethyluroniumhexafluoroalphosphate (HBTU) and 1-hy-

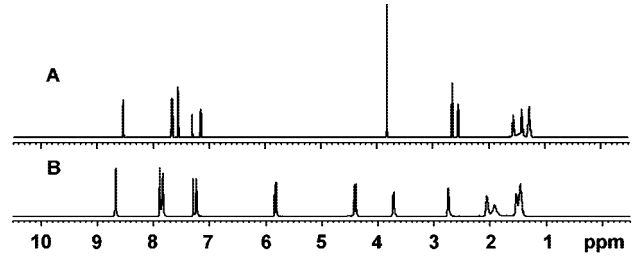

Figure 4. ^{1}H NMR of bis(pyridyl)amine ligand **13** (A) and its Re complex **14** (B) in $CDCl_3$.

(50) Levadala, M. K.; Banerjee, S. R.; Maresca, K. P.; Babich, J.; Zubieta, J. *Synthesis* **2004**, *11*, 1759–1766.

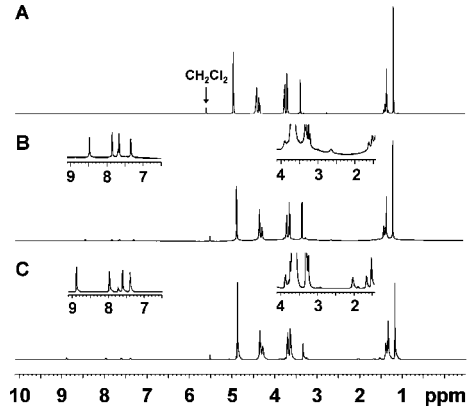

Figure 5. ^{1}H NMR spectra of COOH-G5-$(OH)_{32}$ (A), BisPy-G5-$(OH)_{32}$ (B), and $[ReBisPy-G5-(OH)_{32}]^+$ (C) in CD_3OD. Insets show the aromatic signals of the corresponding spectra in the ranges of 1.5−4.0 and 6.5−9.0 ppm.

droxybenzotriazole (HOBT) as the coupling agents in minimal amounts of DCM. However, subsequent hydrogenolysis to produce the hydroxyl-terminated, ligand-functionalized dendrimer proved problematic. ^{1}H NMR analysis of the product mixture indicated the partial disappearance of aromatic protons, suggesting that the two pyridyl functionalities of ligand **13** are labile under the hydrogenolysis conditions. Considering the difficulty of chromatographically separating high generation dendrimers that differ only at their core, it was deemed futile to attempt purification of the resulting reaction mixture. Instead, the benzylidene protecting groups were first removed to produce the fully deprotected dendrons, and then the core amidation with ligand **13** was performed as the final step in dendrimer synthesis. It was found that amidation proceeded smoothly for COOH-G5-$(OH)_{32}$, COOH-G6-$(OH)_{64}$, and COOH-G7-$(OH)_{128}$ dendrons using HBTU/HOBT as the coupling agents in minimal amounts of dimethylformamide. Surprisingly, even though a large number of peripheral alcohol functionalities are present within the fully deprotected dendrons, each of which can potentially esterify the dendron core under the coupling conditions, no evidence for intramolecular esterification was observed. The primary amine of compound **13** must be sufficiently more nucleophilic that it preferentially reacts with the core acid functionality of the dendrons. Upon purification by preparative gel permeation chromatography using MeOH as the mobile phase, the pure dendrimer products were isolated in typical yields of 60−75%. Unfortunately, all attempts to couple ligand **13** to the eighth-generation dendron, COOH-G8-$(OH)_{256}$, resulted in no detectable conversion to the amide product. The poor reactivity at the G8 stage was attributed to extreme steric hindrance around the core acid functionality caused by the crowded dendrimer periphery.

The coupling of bis(pyridyl)amine ligand **13** to the fully deprotected G5, G6, and G7 dendrons was followed by ^{1}H NMR spectroscopy and MALDI-TOF mass spectometry. Looking at COOH-G5-$(OH)_{32}$ as an example (Figures 5 and 6), successful coupling was evident from the appearance of aromatic signals at 7.33 (2H), 7.66 (2H), 7.85 (2H), and 8.48 (2H) ppm as well as aliphatic proton signals at 1.53 (2H), 1.62 (2H), 3.25 (2H), 3.76 (2H), and 3.87 (4H) ppm (Figure 5B). In addition, a small amide signal at 7.70 ppm can be seen adjacent to the aromatic signal at 7.66 ppm. It should be noted that not all aliphatic peaks were resolved, possibly due to peak broadening as a result of the ligand being coupled to a macromolecular structure with slower relaxation times. The MALDI-TOF mass spectrum for

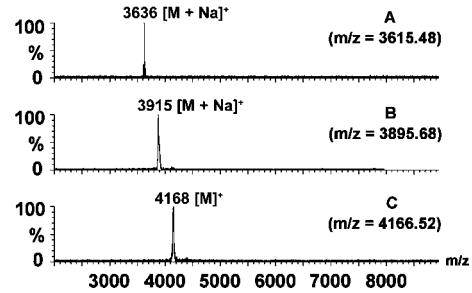

Figure 6. MALDI-TOF MS spectra of COOH-G5-$(OH)_{32}$ (A), BisPy-G5-$(OH)_{32}$ (B), and ReBisPy-G5-$(OH)_{32}$ (C).

BisPy-G5-$(OH)_{32}$ also confirmed the addition of ligand **13**, with a mass increase of 280 Da from the original observed mass (Figure 6). Similar spectral changes were also observed with the G6 and G7 dendrons.

The preparation of a nonradioactive analogue for each of the dendrimer structures to be radiolabeled is important for HPLC analysis of the radioactive products, as retention times of metalated species typically differ from those of unmetalated species. Rhenium is typically used as a nonradioactive standard of ^{99m}Tc due to its virtually identical atomic radius and similar reactivity.[44] Preparation of the nonradioactive Re standards was accomplished by coupling the Re ligand complex **14** using the same chemistry that was demonstrated to work for the unmetalated ligand, producing the desired dendrimers in yields ranging from 55 to 65%. This coupling chemistry was also confirmed by ^{1}H NMR spectroscopy where, in the case of G5, the appearance of the aromatic signals at 7.39 (2H), 7.61 (2H), 7.96 (2H), and 8.89 (2H) ppm, as well as the aliphatic proton signals at 1.55 (4H), 1.69 (2H), 3.25 (2H), and 3.76 (2H) ppm, was observed (Figure 5C). Again, a small amide signal was observed at 7.73 ppm, signifying the formation of the coupled product. Further evidence for the successful preparation of the Re standards came from MALDI-TOF MS, which showed the expected increase of 528 Da as a result of introducing **14**. The MALDI spectrum for the fifth-generation dendrimer, ReBisPy-G5-$(OH)_{32}$, is shown in Figure 6C.

Radiochemistry. The final synthetic step prior to SPECT imaging involved introduction of ^{99m}Tc. Although the aforementioned introduction of Re involved initial metalation of ligand **13**, followed by amidation with the deprotected dendron core, this protocol was less attractive with the ^{99m}Tc radionuclide due to its relatively short half-life. The time required for the amidation and purification procedures would greatly diminish the amount of activity available for testing due to radioactive decay. Furthermore, for future applications involving targeted agents, it is desirable to have the highest possible specific activity, which can be achieved with short synthesis times, as a way to maximize uptake. It was therefore imperative to introduce the ^{99m}Tc in the final step of the synthesis.

The direct labeling was accomplished by first converting sodium pertechnetate ($Na^{99m}TcO_4$) "milked" from the ^{99}Mo/^{99m}Tc-generator to the tris-aqua species $[^{99m}Tc(CO)_3(H_2O)_3]^+$, which bears labile H_2O ligands.[51−53] For this step, we employed

(51) Alberto, R.; Schibli, R.; Egli, A.; Schubiger, A. P.; Abram, U.; Kaden, T. A. *J. Am. Chem. Soc.* **1998**, *120*, 7987–7988.
(52) Alberto, R.; Schibli, R.; Schubiger, A. P.; Abram, U.; Pietzsch, H. J.; Johannsen, B. *J. Am. Chem. Soc.* **1999**, *121*, 6076–6077.
(53) Waibel, R.; Alberto, R.; Willuda, J.; Finnern, R.; Schibli, R.; Stichelberger, A.; Egli, A.; Abram, U.; Mach, J. P.; Pluckthun, A.; Schubiger, P. A. *Nat. Biotechnol.* **1999**, *17*, 897–901.

Scheme 4

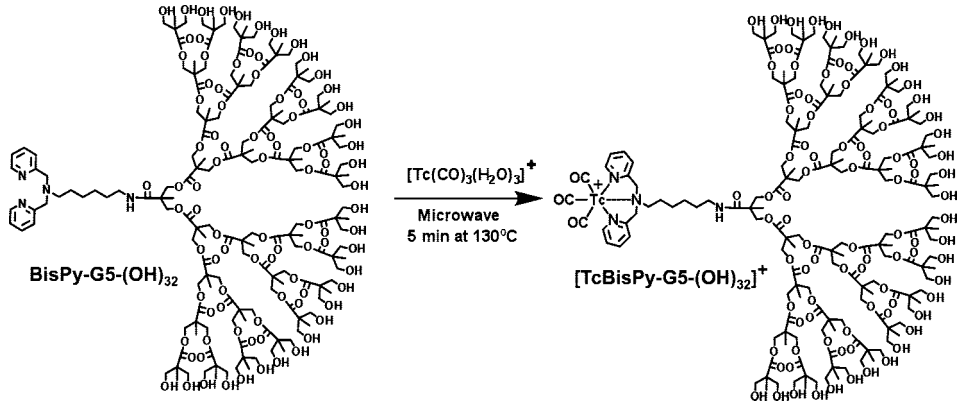

a modified procedure based on the elegant work of Alberto and co-workers,[54] which involved dissolving potassium boranocarbonate ($K_2[BH_3 \cdot CO_2]$), sodium carbonate (Na_2HCO_3), Na/K-tartrate, and borax ($Na_2B_4O_7 \cdot 10H_2O$) in 1 mL of saline solution containing approximately 925 MBq (25 mCi) of $Na^{99m}TcO_4$. The solution was heated by microwave irradiation at 130 °C for 3 min, quantitatively converting the $Na^{99m}TcO_4$ to $[^{99m}Tc(CO)_3(H_2O)_3]^+$. The reaction was cooled and acidified with aqueous HCl to a pH between 4 and 6. An aqueous solution containing 1 mg of the BisPy-G5-$(OH)_{32}$ dendron was added to the reaction vial, and the mixture was again heated by microwave irradiation at 130 °C for an additional 5 min to give $[TcBisPy\text{-}G5\text{-}(OH)_{32}]^+$ (Scheme 4). This entire procedure was completed within 10 min.

Using this protocol, incorporation of ^{99m}Tc within the BisPy-G5-$(OH)_{32}$ dendron to form $[TcBisPy\text{-}G5\text{-}(OH)_{32}]^+$ was accomplished in 89 ± 1% radiochemical yield (RCY) over three labeling experiments. The remaining radioactive material was comprised of unbound $[^{99m}Tc(CO)_3(H_2O)_3]^+$ and ^{99m}Tc loosely bound by the numerous oxygen lone pairs throughout the dendron. Given that it was imperative to isolate each dendron to >99% radiochemical purity in order to produce a viable imaging agent, it was necessary to remove all weakly bound ^{99m}Tc. This was accomplished by adding a large excess of histidine (200 μL of a 10.0 mM solution), which serves as a strongly competing ligand for the weakly bound ^{99m}Tc. The resulting mixture was heated by microwave irradiation to 150 °C for 5 min and then passed through three SEC HiTrap desalting cartridges (GE Healthcare), connected in series, to achieve complete separation of the Tc-labeled high-generation dendrimers from the low-molecular-weight histidine−^{99m}Tc complexes. This procedure enabled the complete removal of all weakly bound ^{99m}Tc species within the sample and allowed isolation of the dendrimers in the required radiochemical purity.

A high-performance liquid chromatograph, equipped with a radioactivity γ detector, was used to monitor the conversion of BisPy-G5-$(OH)_{32}$ to $[TcBisPy\text{-}G5\text{-}(OH)_{32}]^+$. The HPLC chromatograms in Figure 7 show that BisPy-G5-$(OH)_{32}$ had a retention time of 14.66 min, the rhenium standard $[ReBisPy\text{-}G5\text{-}(OH)_{32}]^+$ had a retention time of 16.19 min, and the technetium-labeled dendrimer $[TcBisPy\text{-}G5\text{-}(OH)_{32}]^+$ eluted at 16.49 min. Both BisPy-G5-$(OH)_{32}$ and $[ReBisPy\text{-}G5\text{-}(OH)_{32}]^+$ were monitored using a UV−vis detector, while the $[TcBisPy\text{-}G5\text{-}(OH)_{32}]^+$ was monitored by a gamma detector. The difference of 0.30 min between the rhenium standard, $[ReBisPy\text{-}G5\text{-}(OH)_{32}]^+$, and the radioactive dendrimer, $[TcBisPy\text{-}G5\text{-}(OH)_{32}]^+$, corresponds to the time required to traverse the distance between the UV−vis detector and the gamma detector, which are connected in series. From these data, it is clear that introduction of the radionuclide within the core bis(pyridyl)amine ligand of the G5 dendrimer significantly affects its interaction with the stationary phase, resulting in a large retention time difference. However, the close match between the Re standard and the radiolabeled dendrimer, along with the absence of any other γ-emitting species, confirms that the radiolabeling chemistry is efficient and highly specific to the core ligand.

The radiolabeling conditions developed for G5 were then used to produce $[TcBisPy\text{-}G6\text{-}(OH)_{64}]^+$ and $[TcBisPy\text{-}G7\text{-}(OH)_{128}]^+$ in 70 ± 1% and 53 ± 2% radiochemical yields, respectively (all radiolabeling experiments were performed in triplicate). The structures of these two compounds are given in Figure 8. The decrease in radiochemical yield indicates that accessibility to the bis(pyridyl)amine ligand within the dendron becomes hindered with increasing generation. The HPLC chromatograms for the G6 and G7 ligand-functionalized and radiolabeled dendrimers are given in Figure 9. In the case of G6 (Figure 9A), the unmetalated ligand-bearing dendrimer again had the shortest retention time of 14.77 min, while the ^{99m}Tc-labeled dendrimer appeared at 15.37 min, exactly 0.3 min after the corresponding rhenium standard (data not shown). It should be noted that the retention times of the metalated G6 compounds are more than 1 min shorter than those of the corresponding G5 dendrimers. This indicates that the effect of core metalation on retention time decreases with increasing generation, as would be expected from the enhanced site isolation of the ligand located at the core. This trend continued in the seventh generation, where the retention time of the ^{99m}Tc-labeled

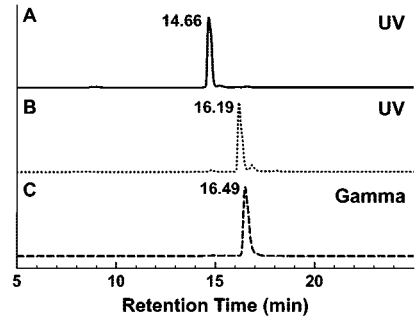

Figure 7. HPLC chromatograms of BisPy-G5-$(OH)_{32}$ (A), $[ReBisPy\text{-}G5\text{-}(OH)_{32}]^+$ (B), and $[TcBisPy\text{-}G5\text{-}(OH)_{32}]^+$ (C).

(54) Alberto, R.; Ortner, K.; Wheatley, N.; Schibli, R.; Schubiger, A. P. *J. Am. Chem. Soc.* **2001**, *123*, 3135–3136.

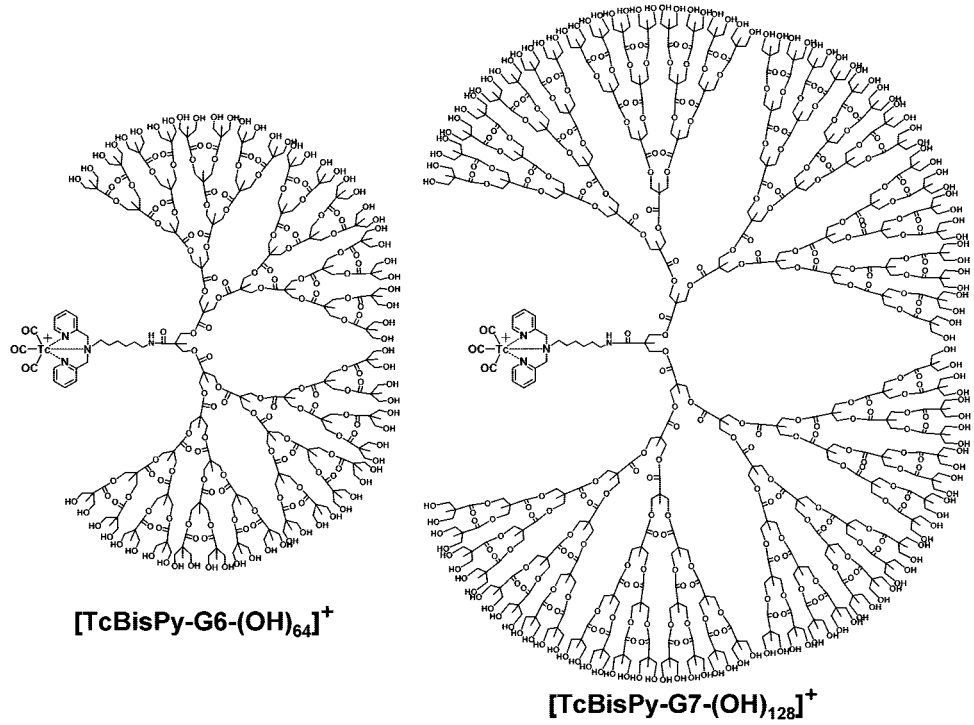

Figure 8. Exact structures of the two highest generation ^{99m}Tc-labeled dendrimers, $[TcBisPy\text{-}G6\text{-}(OH)_{64}]^+$ and $[TcBisPy\text{-}G7\text{-}(OH)_{128}]^+$.

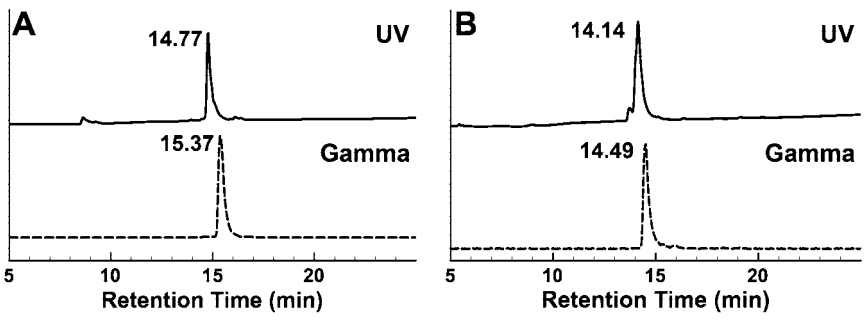

Figure 9. HPLC chromatograms and retention times of (A) BisPy-G6-$(OH)_{64}$ (solid) and $[TcBisPy\text{-}G6\text{-}(OH)_{64}]^+$ (dashed), and (B) BisPy-G7-$(OH)_{128}$ (solid) and $[TcBisPy\text{-}G7\text{-}(OH)_{128}]^+$ (dashed).

dendrimer decreased by almost another minute (Figure 9B). Here the retention time difference between the unmetalated and metalated dendrimers corresponded only to the difference in travel time between the UV−vis and radioactivity detectors, indicating that the actual elution times for the two compounds were practically identical. Figure 10 shows a plot of retention time as a function of dendrimer generation for the unmetalated and radiolabeled dendrimers (before and after correction for the difference in travel time between the two detectors), clearly demonstrating the convergence of retention times at the seventh generation. Again, these differences in retention times indicate that the metalated ligand becomes completely encapsulated within the dendrimer core only at the seventh generation, while at lower generations metalation of the core has an impact on the dendrimer's interactions with its surrounding environment.

Single Photon Emission Computed Tomography (SPECT) Imaging. SPECT imaging was performed using a Gamma Medica Ideas X-SPECT preclinical small-animal imaging system. An aliquot of each of the radiolabeled dendrimers, dissolved in 1 mL of saline solution, was injected into the tail vein of anesthetized adult male Copenhagen rats having an average weight of 275 g. The injected dose amounted to approximately 37 MBq, or 1 mCi, per experiment. The distribution of these dendrimers was monitored using a dual-head detector system equipped with high-resolution parallel beam collimators, having a reconstruction field of view of 125

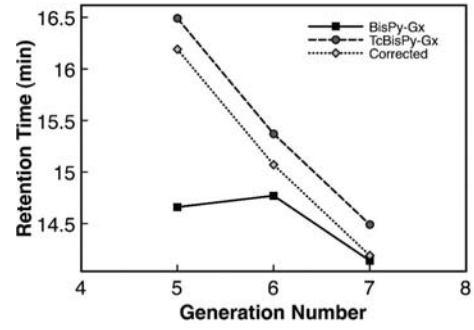

Figure 10. HPLC retention times plotted as a function of dendrimer generation for G5, G6, and G7 dendrimers before (solid line) and after (dashed line) introduction of the radionuclide ^{99m}Tc. The dotted line represents data that have been corrected for the time required to traverse the distance between the UV−vis detector and the gamma detector within the HPLC instrument.

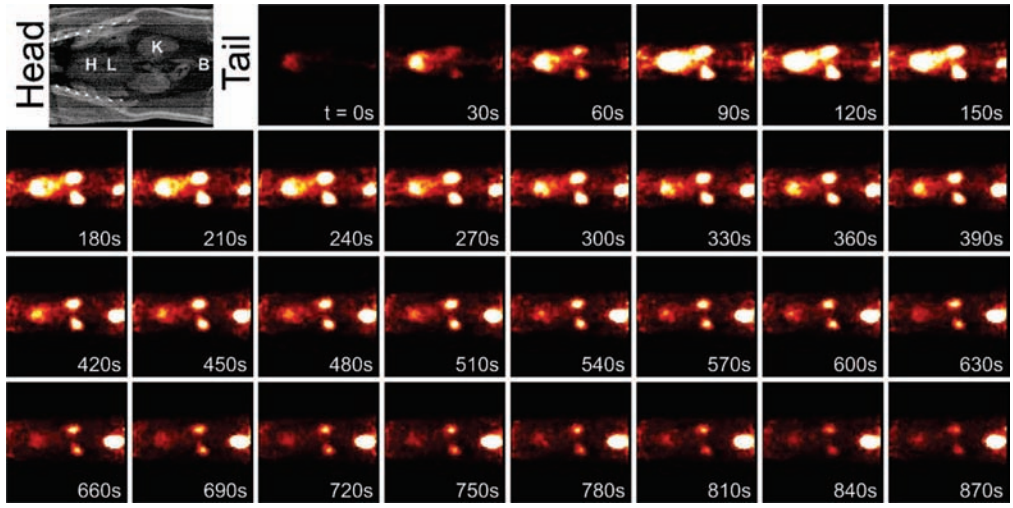

Figure 11. Dynamic SPECT images of $[TcBisPy\text{-}G7\text{-}(OH)_{128}]^+$ taken from time 0 to 15 min with an image every 30 s.

Ⓦ Movie files in AVI format depicting the path of $[TcBisPy\text{-}G7\text{-}(OH)_{128}]^+$, as well as $[TcBisPy\text{-}G5\text{-}(OH)_{32}]^+$ and $[TcBisPy\text{-}G6\text{-}(OH)_{64}]^+$, post injection into the tail vein are available.

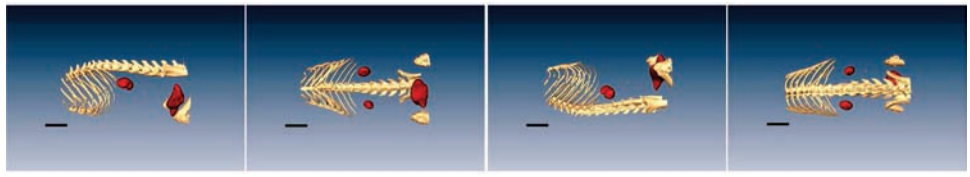

Figure 12. Fused SPECT and CT images of $[TcBisPy\text{-}G7\text{-}(OH)_{128}]^+$ taken over 15 min. Scale bar corresponds to 1 cm.

Ⓦ A complete movie in AVI format of the 360° rotational view is available.

× 125 × 125 mm, with 3−4 mm spatial resolution. Individual images were collected every 10 s for the first 15 min (900 s) of the dynamic scan, followed by one image every 60 s for the next 45 min post injection. The acquired images could be either analyzed individually or assembled into a movie showing the progression of radioactivity as a function of time.

Figure 11 shows the individual SPECT images, at 30 s intervals, from the first 15 min post injection of $[TcBisPy\text{-}G7\text{-}(OH)_{128}]^+$. From these images, the dendritic radiotracer can be seen rapidly moving through the tail vein and immediately into the heart and lungs within the first few seconds of the experiment. Between 30 and 60 s post injection, radiation was observed from the kidneys as the dendrimer begins to be filtered out of the blood. This was almost immediately followed by detection of radioactivity in the bladder (between 120 and 150 s), which served as the final repository of the dendrimer. Very little signal was observed localizing in any other organs or tissues throughout the experiment, with only a low level of highly dispersed radiation across the entire body being detectable. As can be seen from Figure 12, the dendrimer is almost completely removed from the blood within 10 min post injection, and the kidneys transfer it to the bladder almost quantitatively after 15 min. A complete movie of the entire experiment for each injected dendrimer is available online.

The planar dynamic images provide two-dimensional "snapshots" that track the distribution of the dendritic radiotracer across different areas of the animal's body. To visualize the regional and three-dimensional distribution of the dendritic radiotracers, tomographic images were acquired and co-registered with volumetric X-ray computed tomography (CT) data to provide anatomical referencing. Four of these 3-D images, showing the animal's skeleton and locations of highest radioactivity over the course of the first 15 min of the experiment, are depicted in Figure 12 (a complete movie of the 360° rotational view is available online). It is clear from these images that the radioactivity is mainly centered in the kidneys and bladder, with no involvement of any organs that may spatially coincide in the top-down projection (i.e., the liver). These images are therefore consistent with our interpretation of the dynamic SPECT data, where the majority of the radioactivity emanated from the vicinity of the kidneys and the bladder.

Dynamic SPECT images were also collected for the fifth- and sixth-generation dendrimers, $[TcBisPy\text{-}G5\text{-}(OH)_{32}]^+$ and $[TcBisPy\text{-}G6\text{-}(OH)_{64}]^+$, respectively. The individual SPECT images of these molecules are provided in the Supporting Information, and assembled movie files depicting the path of the G5 and G6 molecules post injection into the tail vein are available online. Qualitatively, these data for G5 and G6 are very similar to what is described above for G7. Semiquantitative information was obtained by defining regions of interest (ROIs) on the images and determining the number of counts in that volume. Figure 13 depicts the relative amount of activity measured as a function of time from the ROIs around the heart/lungs, kidneys, and bladder, for each dendrimer generation, normalized to the point of maximum intensity. The nearly exact coincidence of these curves indicates that the path taken by the three dendrimers, from the tail vein to the bladder, was practically identical. The observed rapid clearance of all the dendrimers is likely a result of the molecular weight of each dendrimer (4.1, 7.8, and 15.2 kDa for G5, G6, and G7, respectively) being well below the renal filtration cutoff of 40−60 kDa. Similarly, the measured hydrodynamic radii of these dendrimers, being well below 3 nm, are smaller than the

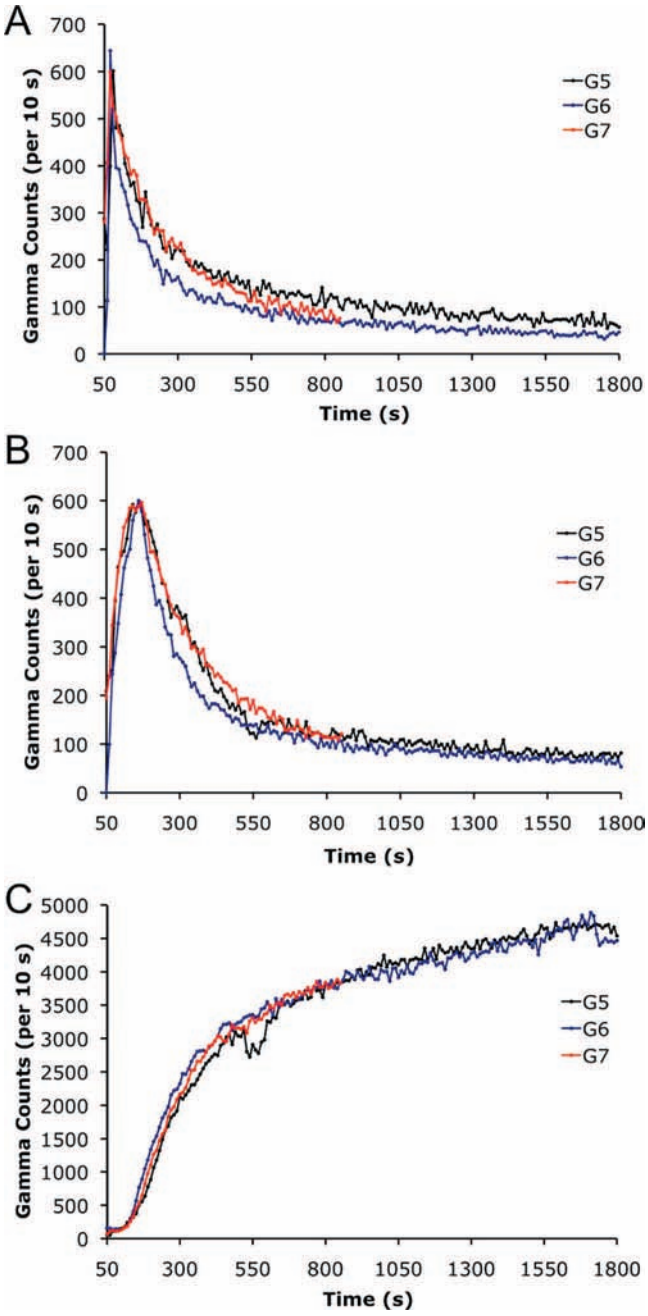

Figure 13. Time−activity plots for γ radiation emanating from the heart/lungs (A), kidneys (B), and bladder (C) for $[TcBisPy\text{-}G5\text{-}(OH)_{32}]^+$ (black curves), $[TcBisPy\text{-}G6\text{-}(OH)_{64}]^+$ (blue curves), and $[TcBisPy\text{-}G7\text{-}(OH)_{128}]^+$ (red curves). For the G7 dendrimer, data were only collected over the first 14 min post injection.

known radius of the renal pores (5 nm),[55] again consistent with the observed rapid clearance. By fitting the decay profiles, from the maximum intensity point onward, to monoexponential decay functions, it was possible to extract an organ clearance half-life ($t_{1/2}$) for the heart/lungs and the kidneys. For all generations, the clearance half-lives were below 150 s (see Supporting Information).

Quantitative Biodistribution Studies. To corroborate and confirm the accuracy of the *in vivo*, real-time data obtained by SPECT analysis, a detailed biodistribution study was performed with the radiolabeled G7 dendrimer, $[TcBisPy\text{-}G7\text{-}(OH)_{128}]^+$. Using the same adult male Copenhagen rats, biodistribution data were collected by harvesting the organs and tissues at 5, 15, 60, 120, and 360 min post injection (5 animals per time point) of the radiolabeled dendrimer administered via the tail vein. The organs/tissues that were harvested from each rat included blood (via heart puncture), heart, lungs, liver, adrenals, kidneys, muscle, stomach, small intestine, cecum, large intestine, testes, brain, bone, adipose tissue, spleen, trachea/thyroid, skin, and eyes. The harvested tissues were weighed, and the radioactivity within each organ/tissue was quantified using a multidetector well counter. The complete data set is presented in Figure 14. These data are in full agreement with the SPECT analysis, indicating that the dendrimer is rapidly cleared from the animals via the kidneys. Greater than 95% of the injected dose is eliminated within the first 5 min, and nearly 99% of the dendrimer is cleared within 15 min. Over the course of the first hour, a small amount of accumulation was found in the digestive tract, including the stomach and small intestine, but these organs showed complete clearance at the 360 min time point. After the full 6 h of the experiment, only traces of radioactivity were found to remain in the animals.

Complete and rapid elimination of molecular imaging and therapy agents from nontarget organs and for drug carriers upon delivery of the therapeutic payload is a critical aspect to their successful clinical implementation. Here, we have demonstrated that it is possible to prepare, characterize, and radiolabel a series of high-generation PMPA dendrimers. Furthermore, it is possible to track these macromolecular radiotracers *in vivo* and in real time using dynamic SPECT imaging, showing that these dendrimer structures are indeed rapidly cleared from the rat bloodstream. Although the short circulation time of the structures investigated here makes them unsuitable for drug delivery applications in their present form, it has already been demonstrated that PEGylation of the PMPA dendrimer periphery dramatically increases blood circulation time.[37] Therefore, these studies serve as the basis for future investigation of analogous dendrimers that will be peripherally modified with agents to improve circulation time (i.e., PEG), as well as to target the dendrimers to specific sites of interest by decoration with a variety of small molecules, sugars, peptides, nucleic acids, and other biologically relevant molecules. Furthermore, the introduction of chemotherapeutic agents within the interior of these structures (carboranes, camptothecin, doxorubicin, etc.), as well as radiotherapeutic agents within the core bis(pyridyl)amine ligand (^{186}Re and ^{188}Re)[56,57] will potentially enable their use in a wide spectrum of therapeutic methodologies.

Conclusion

The preparation of high-generation PMPA dendrons can be accomplished using toluenesulfonyl ethyl ester as an easily removable core protecting group. Removal of the TSe moiety can be accomplished in high yield in dendrons of generations 1 through 8, and cleanly provides dendrons that can be modified at their core carboxylic acid functionality via amidation chemistry. Introduction of a bis(pyridyl)amine ligand allowed the formation of high generation dendrimers that are capable

(55) Deen, W. M.; Bohrer, M. P.; Brenner, B. M. *Kidney Int.* **1979**, *16*, 353–365.
(56) Cyr, J. E.; Pearson, D. A.; Wilson, D. M.; Nelson, C. A.; Guaraldi, M.; Azure, M. T.; Lister-James, J.; Dinkelborg, L. M.; Dean, R. T. *J. Med. Chem.* **2007**, *50*, 1354–1364.
(57) Lambert, B.; de Klerk, J. M. H. *Nucl. Med. Commun.* **2006**, *27*, 223–229.

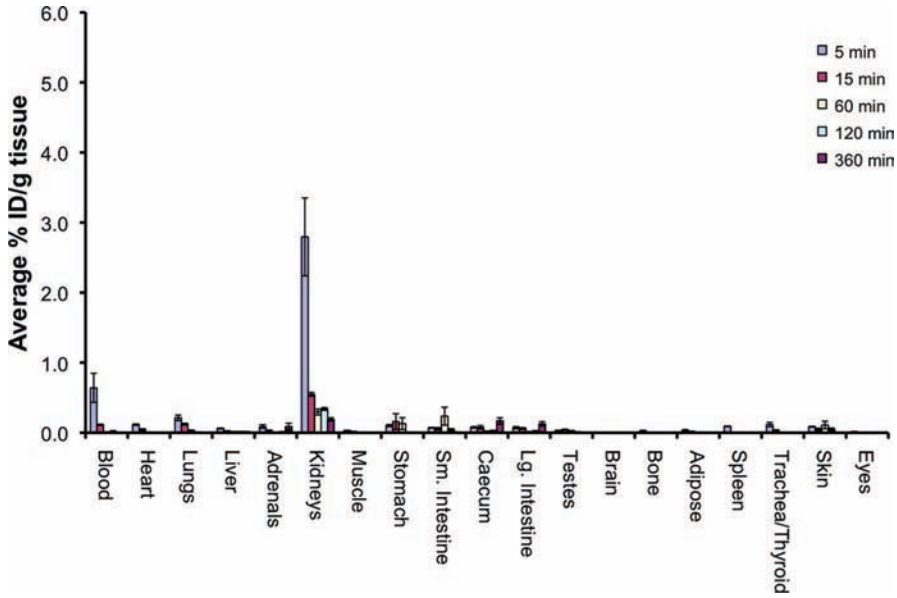

Figure 14. Biodistribution of $[TcBisPy\text{-}G7\text{-}(OH)_{128}]^{+}$ in healthy adult male Copenhagen rats showing percent injected dose (ID) per gram of tissue at five time points post injection: 5, 15, 60, 120, and 360 min (5 animals per time point).

of chelating various isotopes of Tc and Re. Using ^{99m}Tc, radiolabeling conditions were optimized for G5, G6, and G7. It was found that the radiochemical yield decreased with increasing generation, indicating that steric bulk around the core diminishes reactivity. However, the difference in HPLC retention times of the metalated and unmetalated species decreased with generation as a result of improved site isolation of the core functionality. Radiolabeling of the G5−G7 dendrimers with ^{99m}Tc enabled their distribution to be determined noninvasively *in vivo* and in real time. It was found that all three dendrimer generations were rapidly and efficiently removed from the bloodstream via the kidneys and excreted through the bladder within 15 min post injection. The clearance half-lives for the kidneys and heart/lungs were all below 150 s. The SPECT-CT data were corroborated with a quantitative biodistribution study involving *ex vivo* harvesting of various organs and determining the radioactivity within the organs as a function of time. The data from this study indicated rapid clearance through the kidneys, with practically complete elimination of the dendrimers within 15 min. Clearly, this study shows that PMPA dendrimers up to the seventh generation are not retained within any organs of the Copenhagen rats used in this study. The work described here benchmarks the behavior of these dendrons *in vivo* and enables further investigations of their targeting via surface functionalization with a variety of biologically relevant molecules. It also creates a new paradigm for the assessment and optimization of macromolecular-based drug delivery vehicles.

Acknowledgment. We thank Terry Gullon for assistance with biodistribution studies. Financial support for this work was provided by the Natural Science and Engineering Research Council of Canada (NSERC), the Canadian Institutes of Health Research (CIHR), and the Premier's Research Excellence Award (PREA).

Supporting Information Available: Full experimental details and characterization for all compounds. This material is available free of charge via the Internet at http://pubs.acs.org.

JA8078175